J. Phys. D: Appl. Phys. **22** (1989) 1347–1353. Printed in the UK

$Zn_{2x}(CuIn)_yMn_{2z}Te_2$ and $Zn_{2x}(AgIn)_yMn_{2z}Te_2$ alloys

Champa Neal†, John C Woolley†, Rafael Tovar‡ and Miguel Quintero‡

† Ottawa-Carleton Institute of Physics, University of Ottawa, Ottawa, Ontario, Canada K1N 6N5
‡ Centro de Estudios de Semiconductores, Departamento de Física, Facultad de Ciencias, Universidad de Los Andes, Mérida, Venezuela

Received 14 February 1989

Abstract. Polycrystalline samples of $Zn_{2x}(CuIn)_yMn_{2z}Te_2$ and $Zn_{2x}(AgIn)_yMn_{2z}Te_2$ alloys were prepared by a melt and anneal technique. X-ray powder photographs were used to determine equilibrium conditions and lattice parameter values (a and c). In each system, four single-phase fields are found to exist, two with normal zincblende and chalcopyrite structures and two derived from chalcopyrite and zincblende structures in which the Mn atoms show crystallographic ordering on the cation sublattice. In the $Zn_{2x}(AgIn)_yMn_{2z}Te_2$ case, a two-phase (zincblende plus chalcopyrite) field was observed. Optical absorption measurements were carried out to give values of the room temperature optical energy gap E_0 for all single-phase samples. While E_0 varied linearly with composition inside a phase field, the resulting lines had different aiming points at $z = 1.0$. These values of E_0, which are characteristic of the structure, give a good indication of the position of the phase boundaries. Extrapolation to $z = 0$ gave E_0 values of the compounds in the zincblende structure, these being ~0.70 eV for $CuInTe_2$ and ~0.75 eV for $AgInTe_2$.

1. Introduction

Most of the work [1, 2] on semimagnetic semiconductor alloys has been concerned with alloys of the form $II_{1-z}Mn_zVI$. However, similar alloys can be produced from the chalcopyrite I III VI_2 compounds, the ternary analogue of the II VI compounds. The crystallography and optical energy gap values of a number of alloy systems of the form $(IIII)_{1-z}Mn_{2z}Te_2$ have been investigated [3–7] and the work has also been extended to the more general $Cd_{2x}(I\ III)_yMn_{2z}Te_2$ $(x + y + z = 1)$ alloys [3, 4]. The magnetic and ESR results for various $(I\ III)_{1-z}Mn_{2z}Te_2$ alloys have been reported [8].

These chalcopyrite-based alloys are of interest because, depending upon the heat treatment, the alloys can be produced either with the Mn atoms at random on the cation lattice or with the Mn atoms ordered (or partially ordered). The optical energy gap values and the magnetic behaviour are very different in the two different conditions [7, 9]. Before a detailed investigation of effects of Mn ordering can be carried out, a knowledge of the crystallography of the alloy system is required. Most of the work so far has been concerned with the Cd-based alloys [3, 4], with little work on Zn-based materials. Garbato and Ledda [10] investigated the crystallography of the $Zn_{2x}(CuIn)_{1-x}Te_2$ alloys and recently the present authors have presented crystallographic and optical energy gap data for the $Zn_{2x}(AgIn)_{1-x}Te_2$ alloys [11]. In addition, the crystallography, optical energy gap and magnetic behaviour of the $Zn_{1-z}Mn_zTe$ alloys have been studied [12, 13, 14]. In the present work, these investigations of Zn-based alloys are extended to the $Zn_{2x}(CuIn)_yMn_{2z}Te_2$ and $Zn_{2x}(AgIn)_yMn_{2z}Te_2$ alloys.

2. Preparation of samples and experimental measurements

All of the alloys used were produced by the usual melt and anneal techniques [11]. The components of each 1.5 g sample were sealed under vacuum in small quartz ampoules which had previously been carbonised to prevent interaction of the alloy with the quartz, melted together at 1150 °C and then annealed to equilibrium at 600 °C, this choice of annealing temperature being guided by the results for the sections $(AgIn)_{1-z}Mn_{2z}Te_2$ and $(CuIn)_{1-z}Mn_{2z}Te_2$ already investigated [6]. After annealing for 20–30 days to obtain equilibrium at 600 °C, the samples were cooled slowly to room temperature. This treatment was found to give samples in equilibrium at room temperature for all compositions except for those for which a zincblende–chalcopyrite ordering transition occurs at relatively low temperatures. This will be discussed further below. To

0022-3727/89/091347 + 07 $02.50

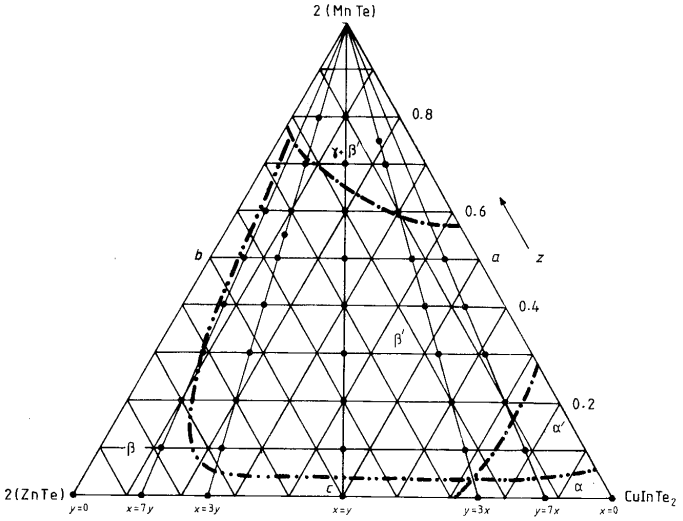

Figure 1. Composition diagram for $Zn_{2x}(CuIn)_yMn_{2z}Te_2$ alloy. ● Samples prepared. Boundaries observed with air-quenched samples: —·—·—, phase boundaries; —··—··—, boundaries between Mn-ordered and Mn-disordered samples.

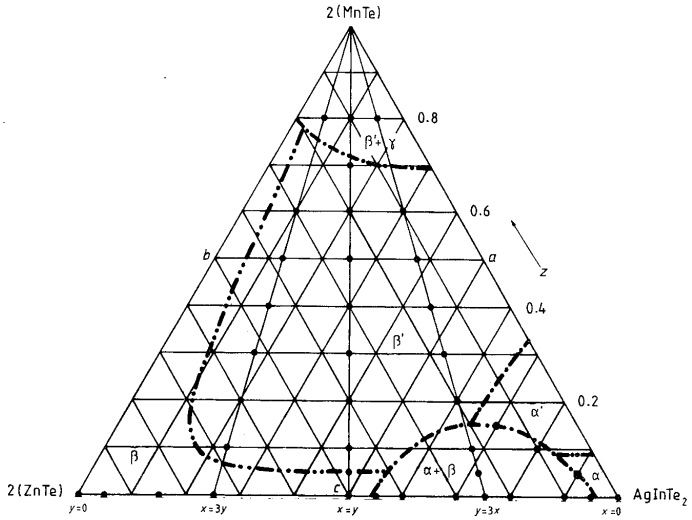

Figure 2. Composition diagram for $Zn_{2x}(AgIn)_yMn_{2z}Te_2$ alloys. ● Samples prepared. Boundaries observed with air-quenched samples: —·—·—, phase boundaries; —··—··—, boundaries between Mn-ordered and Mn-disordered samples.

facilitate comparison of results, samples were made at compositions along the lines in the diagrams at constant x/y ratios, i.e. $y = 0$, $x = 7y$, $x = 3y$, $x = y$, $y = 3x$, $y = 7x$ and $x = 0$, and at various fixed values of z as shown in figures 1 and 2.

X-ray powder photographs, either Guinier or Debye–Scherrer, were used to check the equilibrium conditions of each sample and to determine whether a single-phase form was present. Values of lattice parameters were determined as a function of the composition variables, germanium being used as an internal standard in the Guinier photographs and for chalcopyrite samples for which $c/a \neq 2$.

Slices of each single-phase sample were cut and thinned down to give specimens for standard optical absorption work [15]. Values of $(1/d)\ln(I_0/I_t)$, where d is the thickness, I_0 the incident intensity and I_t the transmitted intensity, were determined as a function of photon energy $h\nu$ and corrected by subtracting a background value to give the absorption coefficient α. It was found that the background absorption in many of these samples was high, so that the slices needed to

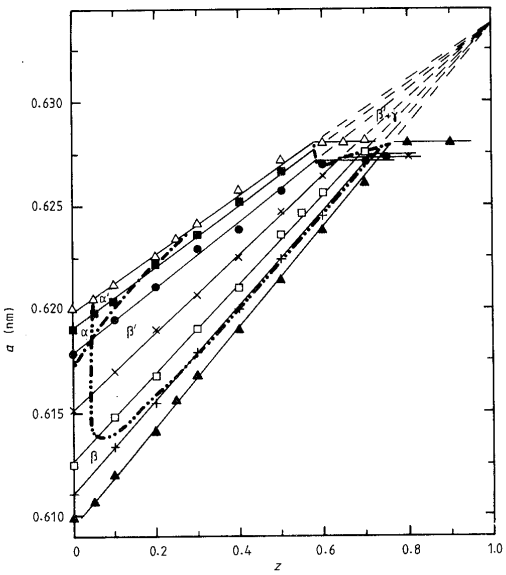

Figure 3. Variation of lattice parameter a with z for various values of x/y in $Zn_{2x}(CuIn)_yMn_{2z}Te_2$. ▲, $y = 0$; +, $x = 7y$; □, $x = 3y$; ×, $x = y$; ●, $y = 3x$; ■, $y = 7x$; △, $x = 0$. —·—·—, observed phase boundaries. —··—··—, observed boundaries between Mn-ordered and Mn-disordered samples.

be ground down to a thickness d of the order of 100 μm or less to obtain any measurable transmitted intensity.

3. X-ray results

In the case of the CuIn alloys, it was found that all samples with lower z values appeared to be single phase, showing the usual lines typical of the zincblende structure of CdTe, while at higher values of z, lines of the NiAs structure of MnTe were observed in addition to the apparent zincblende lines. For all samples, a standard cubic analysis was used to give a value of the lattice parameter corresponding to the zincblende phase, and these values are shown in figure 3 plotted as a function of z for constant x/y ratio. The slope discontinuity in each of these plotted lines gives in the usual manner a point on the boundary of the single-phase field and this boundary is shown in both figures 1 and 3. The values of a for the single-phase samples only are shown plotted as a function of y at constant z in figure 4 where the position of the phase boundary is again indicated.

It is well known [16] that $CuInTe_2$ is tetragonal with $c/a = 2$ and so gives the pseudo-cubic behaviour indicated above. For alloys with high values of y, the usual chalcopyrite ordering lines were observed with relatively low intensity and this intensity decreased as the composition was moved away from $y = 1$. The presence or absence of ordering lines gave an approximate indication of the position of the boundary between the

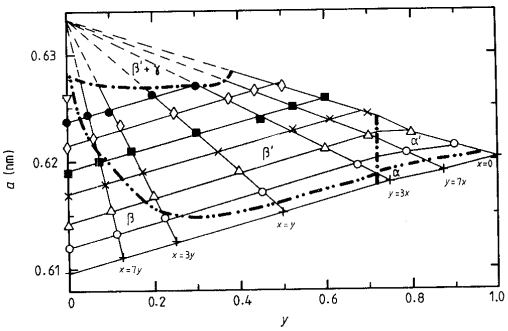

Figure 4. Variation of lattice parameter with y for various values of z in $Zn_{2x}(CuIn)_yMn_{2z}Te_2$. Values of z: +, 0; ○, 0.1; △, 0.2; ×, 0.3; ■, 0.4; ◇, 0.5; ●, 0.6; ▽, 0.7.

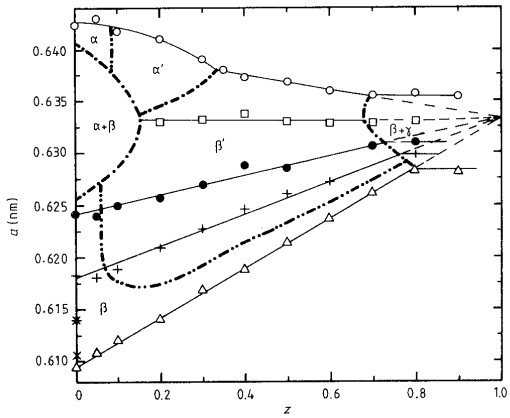

Figure 5. Variation of lattice parameter a with z for various values of x/y in $Zn_{2x}(AgIn)_yMn_{2z}Te_2$. ○, $x = 0$; □, $y = 3x$; ●, $x = y$; +, $x = 3y$; *, $x = 7y$; ×, $x = 9y$; △, $y = 0$.

chalcopyrite (α) and zincblende (β) phase fields. As is seen from figures 3 and 4, a varies linearly with composition in the zincblende field but is non-linear in the chalcopyrite field, a result which has been observed previously in other similar alloy systems [3, 4]. This again allows an estimate to be made of the position of the phase boundary but, as is indicated below, a much better indication of the position of this boundary is obtained from the optical energy gap data. For the zincblende field, the extrapolation of the values of a gives $a = 0.6335$ nm at $z = 1$, in good agreement with previous results [3, 4, 12].

Similar measurements were made for the AgIn alloys. In this case, $c/a \neq 2$ and so the chalcopyrite phase could be more easily observed from splitting of the x-ray lines. Values of the lattice parameter a were again determined for both the zincblende (β) and chalcopyrite (α) phases, and these values are plotted in figures 5 and 6. Again the boundary of the zincblende single-phase field was determined from the slope discontinuities in the graphs of a versus z and

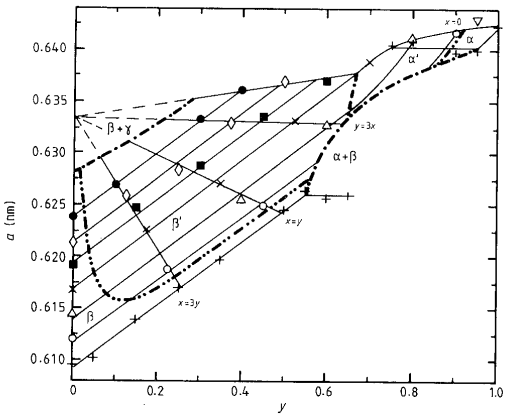

Figure 6. Variation of lattice parameter a with y for various values of z in $Zn_{2x}(AgIn)_yMn_{2z}Te_2$. Values of z: +, 0; ▽, 0.05; ○, 0.1; △, 0.2; ×, 0.3; ■, 0.4; ◇, 0.5; ●, 0.6. —·—·—, observed phase boundaries. —··—··—, observed boundaries between Mn-ordered and Mn-disordered samples.

this boundary is shown in figures 2, 5 and 6. In contrast to the CuIn case, a two-phase ($\alpha + \beta$) field was clearly observed in the composition range indicated in figure 5. For these alloys, the chalcopyrite (α) and zincblende (β) phases clearly showed different lattice parameter values. This miscibility gap was previously observed for the line $z = 0$ [11], and as in that case, the lattice parameter values showed that the tie-lines of this two-phase field did not lie in the plane of the diagram being investigated. Because of the limited range of the chalcopyrite single-phase condition in this case, values for the chalcopyrite lattice parameters were obtained only for the line $x = 0$. As indicated above, again the variation of a with z for the chalcopyrite phase was non-linear, but in the zincblende field a linear variation was found, again extrapolating to a value of $a = 0.6333$ nm at $z = 1$. As shown previously [4], in the chalcopyrite range, the value of c/a varied from 1.9 at $z = 0$ to a value of 2 at $a = 0.33$. Because of the limited information on the chalcopyrite field, the boundary between the α and β fields and those between the ($\alpha + \beta$) and the single-phase α and β fields, shown in figures 2, 5 and 6, are estimates only.

When the AgIn and CuIn diagrams are compared, it is seen that while the AgIn diagram clearly shows a two-phase ($\alpha + \beta$) field with α and β phases having different values for a, for the CuIn case the lattice parameter values appear to indicate that for each alloy a single value of a is obtained with no two-phase range. However, the results of Garbato and Ledda [10] for the section $Zn_{2x}(CuIn)_{1-x}Te_2$ indicate that a two-phase range occurs, extending at 400 °C from $x = 0.09$ to $x = 0.28$. However, the values of lattice parameter given indicate that at each value of x in that range, the chalcopyrite and zincblende phases show the same value of a. In that work, the presence of both zincblende and chalcopyrite phases was detected by intensity measurements using an x-ray diffractometer. In the present work, the standard x-ray film methods used were insufficiently sensitive to show the presence of the two phases of equal lattice parameter in this way.

This condition, when both chalcopyrite and zincblende phases are present with equal a values and hence the same composition, has also been observed for the alloys $Zn_{2x}(CuGa)_{1-x}Te_2$ [17] and $(AgGa)_{1-z}Mn_{2z}Te_2$ [7]. The problem of detecting the simultaneous occurrence of a zincblende and a chalcopyrite phase with equal values of the lattice parameter a is simplified for the case when $c/a \neq 2$. For $CuGaTe_2$ ($c/a = 1.98$) and $AgGaTe_2$ ($c/a = 1.965$), the chalcopyrite lines are split and, for example, the lines of the 220 and 204 pair and of the 312 and 116 pair can be observed separately. Since the zincblende 220 and 311 lines practically coincide with the chalcopyrite 220 and 312 lines, measurements of the relative intensity of 220 to 204 and 312 to 116 can give a good estimate of the relative amounts of zincblende and chalcopyrite phases present. Ledda [18] has found that when $Zn_{2x}(CuGa)_{1-x}Te_2$ alloys in the appropriate composition range are annealed at low temperatures (~200 °C), the relative amount of chalcopyrite to zincblende slowly increases with time of anneal. These various results indicate that the apparent two-phase behaviour in the $Zn_{2x}(CuIn)_{1-x}Te_2$ [10] and $Zn_{2x}(CuGa)_{1-x}Te_2$ [17] phase diagrams is due to an order–disorder reaction which is slow because of the relatively low ordering temperature. The range of composition at any temperature in which both zincblende and chalcopyrite phases will be present in equilibrium will be quite small, being determined by the curve giving degree of order against temperature. However, with the low ordering temperatures occurring in some of these alloys, it is very difficult to obtain the equilibrium condition. For non-equilibrium samples the composition range over which the two phases are simultaneously observed can be appreciably larger than the equilibrium range.

One other difference between the data of Garbato and Ledda and the present results for $Zn_{2x}(CuIn)_{1-x}Te_2$ alloys is the variation of lattice parameter with x. The two sets of data show good agreement in the zincblende range but show some divergence for the chalcopyrite alloys. The maximum difference occurs for $CuInTe_2$, where the present value of $a = 0.6202$ nm is to be compared with 0.6179 nm [10]. As has been suggested previously [3, 4], such a difference in the value of the lattice parameter for these chalcopyrite compounds can be attributed to different degrees of non-stoichiometry in the samples, which depend upon the particular method of preparation.

4. Optical energy results

Optical absorption measurements were made on all of the samples which appeared single phase from the x-

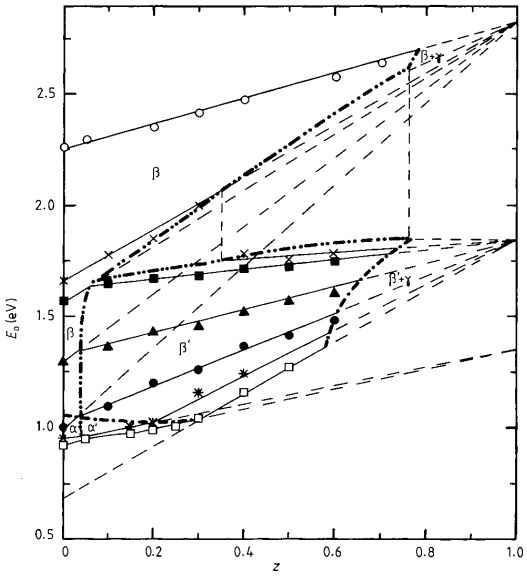

Figure 7. Variation of room temperature optical energy gap E_0 with z for various values of x/y in $Zn_{2x}(CuIn)_yMn_{2z}Te_2$. ○, $y = 0$; ×, $x = 7y$; ■, $x = 3y$; ▲, $x = y$; ●, $y = 3x$; *, $y = 7x$; □, $x = 0$. —·—·—, observed phase boundaries. —··—··—, observed boundaries between Mn-ordered and Mn-disordered samples.

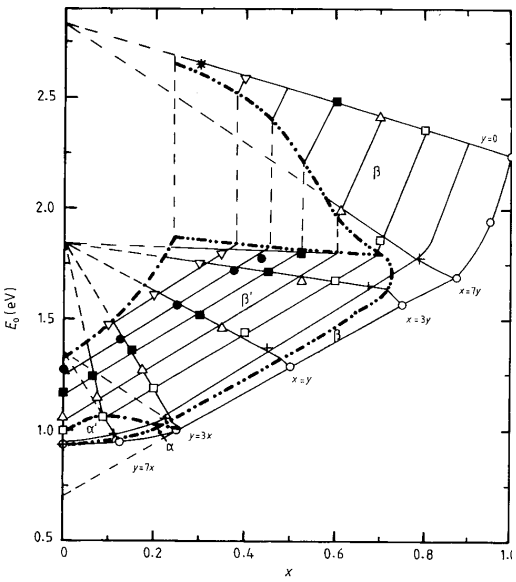

Figure 8. Variation of room temperature optical energy gap E_0 with x for various values of z in $Zn_{2x}(CuIn)_yMn_{2z}Te_2$. Values of z: ○, 0; +, 0.1; □, 0.2; △, 0.3; ■, 0.4; ●, 0.5; ▽, 0.6; *, 0.7. —·—·—, observed phase boundaries. —··—··—, observed boundaries between Mn-ordered and Mn-disordered samples.

ray photographs. It is well known that ZnTe and both chalcopyrite compounds, $CuInTe_2$ and $AgInTe_2$, are direct-gap semiconductors and previous work [3, 4, 12] has shown that the alloys $Zn_{1-z}Mn_zTe$, $(CuIn)_{1-z}Mn_{2z}Te_2$ and $(AgIn)_{1-z}Mn_{2z}Te_2$ also have direct gaps. Therefore here, plots of $(\alpha h\nu)^2$ versus $h\nu$ were used in all cases to determine the optical energy gap E_0 values, in each case the higher values of $(\alpha h\nu)^2$ being linearly extrapolated to zero to give a value of E_0. The resulting variation of E_0 for the CuIn alloys is shown in figure 7 as a function of z and as a function of x at constant z in figure 8. The corresponding data for the AgIn alloys are shown in figures 9 and 10.

It has been shown in previous work on alloy systems of this type [3, 4, 7] that E_0 varies linearly with z inside any given field and that the aiming point of the E_0 versus z line at $z = 1$ is characteristic of the structure concerned. This parameter takes the following values: for Mn-disordered zincblende 2.85 eV; for Mn-ordered zincblende 1.9 eV; and for Mn-ordered chalcopyrite 1.35 eV. For the case of Mn-disordered chalcopyrite, the range of composition available is small and so no accurate determination of the aiming point values has so far been made, but the value lies somewhere between 2.2 and 2.85 eV [19]. In figures 7 and 9, it is seen that the values of E_0 in the Mn-ordered zincblende and chalcopyrite fields of the present alloys are in good agreement with these previous values. It is to be noted that these alloys will give the E_0 value for the Mn-ordered phase even if the method of preparation is such that some of the high-temperature Mn-disordered phase is still present. This is because the E_0 value of the ordered phase in all cases is lower than that of the disordered phase, and so in the optical absorption measurements the absorption edge of the ordered phase occurs at lower energies and completely masks the edge corresponding to the disordered phase. These E_0 aiming-point values can be used to determine or confirm the position of the boundaries between the various fields. Thus in figure 7, for the CuIn alloys, for the lines $y = 3x$, $x = y$ and $x = 3y$ and $z > 0.1$, the experimental points lie on straight lines which extrapolate to $E_0 = 1.85$ eV at $z = 1.0$, in good agreement with the value given above. If the values of E_0 on the $z = 0$ line for $y = 3x$, $x = y$ and $x = 3y$ are joined to the value of 2.85 eV at $z = 1.0$ as shown in the figure, the points of intersection of these lines with those through the corresponding experimental points for $z = 0.1$ give a good indication of the boundary between the Mn-disordered and Mn-ordered fields. A similar construction has been carried out in figure 8 to give the boundary between the Mn-ordered chalcopyrite and Mn-ordered zincblende fields. The positions of these boundaries are shown in figure 1. These boundary estimates are approximate in that they assume that E_0 is the same on both sides of the boundary, which need not be the case. Inspection of the E_0 graphs for the cases of $y = 3x$, $x = y$ and $x = 3y$ indicates that the error in these estimates should not exceed ± 0.05 in composition.

In the case of the $x = 7y$ line, the results are quite different. In this case, the E_0 values for $z < 0.3$ lie on a straight line extrapolating to $E_0 = 2.85$ eV at $z =$

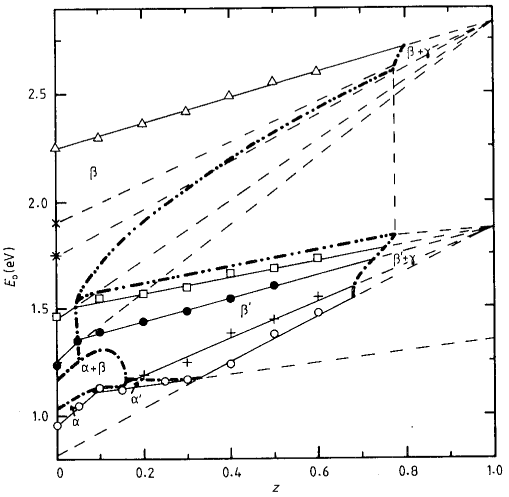

Figure 9. Variation of room temperature energy gap E_0 with z for various values of x/y in $Zn_{2x}(AgIn)_yMn_{2x}Te_2$. ○, $x = 0$; +, $y = 3x$; ●, $y = x$; □, $x = 3y$; *, $x = 7y$; ×, $x = 9y$; △, $y = 0$. —·—·—, observed phase boundaries. —··—··—, observed boundaries between Mn-ordered and Mn-disordered samples.

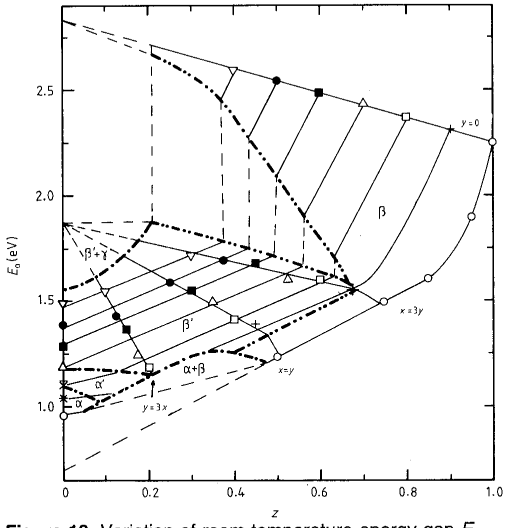

Figure 10. Variation of room temperature energy gap E_0 with x for various values of z in $Zn_{2x}(AgIn)_yMn_{2z}Te_2$. Values of z: ○, 0; *, 0.05; +, 0.1; ×, 0.15; □, 0.2; △, 0.3; ■, 0.4; ●, 0.5; ▽, 0.6. —·—·—, observed phase boundaries. —··—··—, observed boundaries between Mn-ordered and Mn-disordered samples.

1.0, indicating a Mn-disordered zincblende structure. However, for $z > 0.4$, the E_0 values lie on a straight line extrapolating to 1.85 eV at $z = 1.0$ indicating a Mn-ordered zincblende. The boundary between the Mn-ordered and Mn-disordered structures lies between $z = 0.3$ and $z = 0.4$ and the discontinuity in E_0 at this boundary is approximately 0.3 eV as is shown in figure 7. Thus, the single line used to indicate the Mn-disordered–Mn-ordered boundary up to the line $x = 3y$ has to be drawn as two diverging lines as the x/y ratio is further increased. The area between the two lines represents pairs of z, E_0 values which cannot occur, and this area is indicated in figure 7. Strictly, of course, this region extends along the whole of the boundary but is very narrow for the lower x/y ratios. The same information is shown plotted in a different way in figure 8. Again the boundary has to be split into two lines for $x/y > 4$.

Another result of interest which can be obtained from figure 7 and 8 is a value of E_0 for $CuInTe_2$ in the zincblende form. This is given by the extrapolation to $z = 0$ of the values of E_0 in the zincblende field for the $x = 0$ line as indicated in figure 7, or by extrapolation to $x = 0$ of the values in the zincblende field for the $z = 0$ line, as in figure 8. The extrapolated value for $CuInTe_2$ obtained in this way is $E_0 \sim 0.70$ eV.

Figures 9 and 10 show a corresponding set of data for the AgIn alloys and the same method of analysis was used as for the CuIn alloys. The boundaries between the various Mn-disordered and Mn-ordered fields have been estimated and are shown on both figures. In this case, alloys for the line $x = 7y$ were not investigated and the energy discontinuity at the Mn-disordered to Mn-ordered transition for $x/y > 4$ is a rough estimate only. The extrapolations to $AgInTe_2$ give a value of E_0 for the zincblende structure of ~0.75 eV in this case.

5. Discussion

A wide range of solid solubility in the zincblende and chalcopyrite phases is observed in these $Zn_{2x}(CuIn)_yMn_{2z}Te_2$ and $Zn_{2x}(AgIn)_yMn_{2z}Te_2$ alloys, similar to the results for the corresponding Cd-based alloys. However, the $Zn_{2x}(AgIn)_yMn_{2z}Te_2$ alloys show a relatively wide miscibility gap between chalcopyrite and zincblende at low z, consistent with the previous results shown for the $Zn_{2x}(AgIn)_{1-x}Te_2$ alloys [11]. The miscibility gap previously reported by Garbato and Ledda [10] for the $Zn_{2x}(CuIn)_{1-x}Te_2$ alloys would appear to be due to a low-temperature order–disorder reaction, chalcopyrite–zincblende, where the very small diffusion rates at low temperatures makes it very difficult to obtain samples in thermal equilibrium. The same effect must apply in the $Zn_{2x}(CuIn)_yMn_{2z}Te_2$ alloys, but it is difficult to investigate since the zincblende and chalcopyrite phases show, at any given composition, practically the same lattice parameter value a.

The effects of Mn ordering are observed for both the chalcopyrite and zincblende phases with the value of E_0 at any given composition depending upon whether the phase is Mn-ordered or Mn-disordered. The extrapolation of the E_0 values to $z = 1.0$ for any given x/y ratio gives limiting values of E_0 in good agreement with those obtained previously for the Cd-

based alloys.

Extrapolations to $z = 0$ for the $x = 0$ lines and to $x = 0$ for the $z = 0$ lines gives values of E_o for the compounds $CuInTe_2$ and $AgInTe_2$ in the zincblende form of ~0.70 and ~0.75 eV respectively. Previously, similar values have been obtained for other alloy systems [6, 7, 9, 20] and corresponding values obtained for the $AgGaTe_2$ [7], $CuGaTe_2$ [20] and $CuInSe_2$ [9] compounds. These results indicate that, for this set of compounds, the difference between the measured E_o for the chalcopyrite form and the extrapolated E_o for the zincblende form is of the order of 0.25 eV in each case. Various theoretical studies have been made to estimate the value of this difference (ΔE_o) for the different chalcopyrite compounds. Thus Zunger [21] indicates that $\Delta E_o = 0.4$ eV for most of these compounds while Rincón [22] predicts values lying in the range 0.42–0.50 eV for the above four compounds. The values estimated by the present extrapolation technique are smaller than these theoretically proposed values.

Acknowledgments

The authors wish to thank Professor L Garbato and Professor F Ledda of Instituto di Fisica dell' Universita Cagliari, Italy and Professor C Rincón of Universidad de Los Andes, Mérida, Venezuela, for useful discussions. They are also grateful to Mr G S Perez and Mr F Sánchez for technical assistance. The Venezuelan authors wish to thank Consejo de Desarrollo Cientifico Humanistico y Tecnológico (CDCHT) and Consejo Nacional de Investigaciones Científicas y Tecnologicas (CONICIT) Venezuela for financial support. Thanks also to Mrs Margarita de Quintero for typing the manuscript.

References

[1] Gai J A 1980 *J. Phys. Soc. Japan* **49** 797
[2] Furdyna J K 1982 *J. Appl. Phys.* **53** 7637
[3] Quintero M, Dierker L and Woolley J C 1986 *J. Solid State Chem.* **63** 110
[4] Quintero M and Woolley J C 1985 *Phys. Status Solidi* a **92** 449
[5] Aresti A, Garbato L, Geddo-Lehmann A and Manca P 1986 *Proc. 7th Int. Conf. on Ternary and Multinary Compounds* (Pittsburg: Materials Research Society) p 497
[6] Quintero M, Grima P, Tovar R, Perez G S and Woolley J C 1988 *Phys. Status Solidi* a **107** 205
[7] Quintero M, Tovar R, Al-Najjar M, Lamarche G and Woolley J C 1988 *J. Solid State Chem.* **74** 136
[8] Woolley J C, Lamarche G, Manoogian A, Quintero M, Dierker L, Al-Najjar M, Proulx D, Neal C and Goudreault R 1986 *Proc. 7th Int. Conf. on Ternary and Multinary Compounds* (Pittsburg: Materials Research Society) p 479
[9] Quintero M, Grima P, Avon J E, Lamarche G and Woolley J C 1988 *Phys. Status. Solidi* a **108** 794
[10] Garbato L and Ledda F 1979 *J. Solid State Chem.* **30** 189
[11] Tovar R, Quintero M, Grima P and Woolley J C 1989 *Phys. Status Solidi* a **111** 405
[12] Brun del Re B, Donnofrio R, Avon J E, Majid J and Woolley J C 1983 *Nuovo Cimento* D **2** 1911
[13] Donofrio T, Lamarche G and Woolley J C 1985 *J. Appl. Phys.* **57** 1932
[14] Donofrio T, Lamarche G and Woolley J C 1985 *J. Appl. Phys.* **57** 1937
[15] Goodchild R G, Hughes O H, Lopez-Rivera S A and Woolley J C 1982 *Can. J. Phys.* **60** 1096
[16] Shay J P and Wernick G H 1975 *Ternary Chalcopyrite Semiconductors* (New York: Pergamon) pp 4, 110
[17] Casula F and Mula G 1983 *Nuovo Cimento* D **6** 1650
[18] Ledda F private communication
[19] Quintero M, Grima P, Guerrero E, Tovar R, Perez G S and Woolley J C 1988 *J. Solid State Chem.* **77** 26
[20] Quintero M, Grima P, Tovar R, Goudreault R, Bissonnette D, Lamarche G and Woolley J C 1988 *J. Solid State Chem.* **76** 210
[21] Zunger A 1987 *Appl. Phys. Lett.* **50** 164
[22] Rincón C 1987 *Solid State Commun.* **64** 663